Published in final edited form as:
Int J Parasitol. 2007 January ; 37(1): 33–51. doi:10.1016/j.ijpara.2006.10.003.

Enzymes of type II fatty acid synthesis and apicoplast differentiation and division in *Eimeria tenella*⋆

D.J.P. Ferguson[a,*], **S.A. Campbell**[b,1], **F.L. Henriquez**[b,2], **L. Phan**[c], **E. Mui**[c], **T.A. Richards**[d], **S.P. Muench**[e], **M. Allary**[f], **J.Z. Lu**[f], **S.T. Prigge**[f], **F. Tomley**[g], **M.W. Shirley**[g], **D.W. Rice**[e], **R. McLeod**[c], and **C.W. Roberts**[b]

[a] Nuffield Department of Pathology, University of Oxford, John Radcliffe Hospital, Oxford OX3 9DU, UK

[b] Department of Immunology, University of Strathclyde, Glasgow G4 0NR, UK

[c] Department of Ophthalmology and Visual Sciences, Pediatrics (Infectious Diseases), Pathology and Committees on Genetic, Molecular Medicine, and Immunology, University of Chicago, Chicago, IL 60637, USA

[d] School of Biosciences, University of Exeter, Geoffrey Pope Building, Stocker Road, Exeter EX4 4QG, UK

[e] Department of Molecular Biology and Biotechnology, The University of Sheffield, Sheffield S10 2TN, UK

[f] School of Public Health, Johns Hopkins University, Baltimore, MD 21205, USA

[g] Division of Molecular Biology, Institute of Animal Health, Compton, Newbury, Berkshire RG20 7NN, UK

Abstract

Apicomplexan parasites, *Eimeria tenella*, *Plasmodium* spp. and *Toxoplasma gondii*, possess a homologous plastid-like organelle termed the apicoplast, derived from the endosymbiotic enslavement of a photosynthetic alga. However, currently no eimerian nuclear encoded apicoplast targeted proteins have been identified, unlike in *Plasmodium* spp. *and T. gondii*. In this study, we demonstrate that nuclear encoded enoyl reductase of *E. tenella* (*Et*ENR) has a predicted N-terminal bipartite transit sequence, typical of apicoplast-targeted proteins. Using a combination of immunocytochemistry and EM we demonstrate that this fatty acid biosynthesis protein is located in the apicoplast of *E. tenella*. Using the *Et*ENR as a tool to mark apicoplast development during the *Eimeria* lifecycle, we demonstrate that nuclear and apicoplast division appear to be independent events, both organelles dividing prior to daughter cell formation, with each daughter cell possessing one to four apicoplasts. We believe this is the first report of multiple apicoplasts present in the infectious stage of an apicomplexan parasite. Furthermore, the microgametes lacked an identifiable apicoplast consistent with maternal inheritance via the macrogamete. It was found that the size of the organelle and the abundance of *Et*ENR varied with developmental stage of the *E. tenella* lifecycle. The high levels of *Et*ENR protein observed during asexual development and macrogametogony is potentially associated with the increased synthesis of fatty acids required for the rapid formation of numerous merozoites and for the extracellular development and survival of the oocyst. Taken

⋆Nucleotide sequences reported in this paper are available in the GenBank database under the accession number AY566297.

*Corresponding author. Tel.: +44 1865 220 514; fax: +44 1865 228 980. david.ferguson@ndcls.ox.ac.uk (D.J.P. Ferguson).
[1]Present address: School of Life Sciences, Faculty of Health and Life Sciences, Napier University, Edinburgh, UK.
[2]Present address: School of Engineering and Science, University of Paisley, Paisley, Scotland, UK.

together the data demonstrate that the *E. tenella* apicoplast participates in type II fatty acid biosynthesis with increased expression of ENR during parasite growth. Apicoplast division results in the simultaneous formation of multiple fragments. The division mechanism is unknown, but is independent of nuclear division and occurs prior to daughter formation.

Keywords

Eimeria tenella; Apicoplast; Enoyl reductase; Immunocytochemistry; Stage specific expression

1. Introduction

The group of parasites forming the Apicomplexa contains numerous and diverse parasitic forms of medical and veterinary importance (Fast et al., 2002). The significance of *Plasmodium* spp. (malaria causes two million childhood deaths per year) and *Toxoplasma gondii* (two billion chronically infected individuals) as human pathogens are well known (Ferguson, 2002; Snow et al., 2005). *Eimeria* spp. are important pathogens in domestic animals being associated with losses of approximately two billion dollars per year in the poultry industry of the USA alone (Wallach, 2002). It is such a serious and intractable problem that commercial poultry food contains drugs to control the infection. Apicomplexan parasites are characterised by a set of organelles (rhoptries, micronemes and dense granules) located in the apical cytoplasm (Levine et al., 1980). However, an additional organelle, found in many members of this phylum, is the apicoplast. The consensus is that this organelle is the plastid remnant of an endosymbiont although the exact origin is still the subject of debate (reviewed Wilson, 2002; Waller and McFadden, 2005). Studies using in situ hybridisation, have demonstrated the presence of a multi-membraned (four unit membranes) organelle present in the peri-nuclear cytoplasm of *T. gondii* with a 35 kb circular genome (Kohler et al., 1997; McFadden and Waller, 1997). Thus the apicoplast is different from the other DNA-containing organelle, the mitochondrion, which is encapsulated by two membranes. The apicoplast had previously been identified as a distinct organelle by EM and termed the Golgi adjunct in *T. gondii* (Sheffield and Melton, 1968) or the multi-membranous organelle in *Eimeria* species (Ferguson et al., 1976). The presence of multiple (four) membranes is believed to be the consequence of the secondary endosymbiotic event (Kohler et al., 1997; Cavalier-Smith, 2000). Although the apicoplast has its own small genome, many of the apicoplast-specific proteins are coded by genes located in the nucleus, which are subsequently transferred into the apicoplast (Waller et al., 1998). The functions of the apicoplast are still incompletely understood, but it is known to be involved in type II fatty acid synthesis and isoprenoid biosynthesis in *T. gondii* plus heme biosynthesis in *Plasmodium* spp. (Waller et al., 1998; Zuther et al., 1999; McLeod et al., 2001; Surolia and Surolia, 2001; Wilson, 2002; Roberts et al., 2003; Ralph et al., 2004; Waller and McFadden, 2005).

To date, studies of the apicoplast have been limited to the in vitro proliferative form (tachyzoite) of *T. gondii*, the erythrocytic stages of *P. falciparum* and the asexual multiplication of *Sarcocystis neurona* (reviewed Vaishnava and Striepen, 2006). In addition, stage specific variations during in vivo development of *T. gondii* in both the intermediate and final hosts have been described (Ferguson et al., 2005). Recently, the *E. tenella* apicoplast genome has been sequenced (Cai et al., 2003). However, to date no nuclear encoded, apicoplast localised proteins have been identified and little is known about the development or division of the apicoplast in *Eimeria* spp. during a lifecycle that has many different developmental stages.

In the present study, we have examined the *E. tenella* genome database (www.sanger.ac.uk/Projects/E_tenella/) to identify the genes involved in type II fatty acid synthesis. Enoyl reductase was identified, sequenced and expressed as a recombinant protein.

Antibodies to the recombinant enoyl reductase of *E. tenella* (*Et*ENR), raised in mice, were employed using light and EM immunocytochemical techniques to study the location of the apicoplast and also the relative level of expression of *Et*ENR during in vivo development. This was correlated with detailed ultrastructural studies of the apicoplast and its division during asexual and sexual development.

2. Materials and methods

2.1. Parasites

The Houghton strain of *E. tenella* was used in this study.

2.2. Identification of genes involved in type 2 fatty acid synthesis

The *E. tenella* genome project was searched for enzymes involved in type II fatty acid synthesis. Preliminary data was obtained from the *E. tenella* genome sequencing project (Wellcome Trust Sanger Institute http://www.sanger.ac.uk/cgi-bin/blast/submitblast/e_tenella/omni). Using the tBLASTn algorithm, the genome was interrogated with known enzyme amino acid sequences to identify DNA sequences containing potential coding regions homologous to the enzymes (acetyl-coA carboxylase, acetyl-CoA-ACP transacylase, malonyl-CoA-ACP transacylase [ACAT], β-ketoacyl-ACP synthase [β-KAS], β-ketoacyl-ACP reductase [β-KAR], β-hydroxyacyl-ACP dehydrase [β-HAD] and enoyl-ACP reductase [ENR]).

2.3. Cloning, expression and purification of recombinant EtENR

RNA was extracted from sporozoite stage *E. tenella* W15 parasites using RNAeasy Maxi kit (Qiagen, Crawley, UK) as per the manufacturer's instructions and used to generate cDNA using Superscript III reverse transcriptase (Invitrogen, Paisley, UK) as per the manufacturer's instructions.

The coding sequence of *E. tenella* ENR was amplified from cDNA using the following primers *Et*ENR for 5′ GTGTCGGCTGTCACCTCC3′ and *Et*ENRrev 5′ CTCAAGGGGTGAGGGACTTG3′. PCR reactions were performed in a volume of 25 μl and contained a final concentration of 1× ReddyMix™ PCR Mastermix with 1.5 mM $MgCl_2$ (ABgene) and 25 pM of each primer. PCR products were separated on a 1% agarose gel and visualised by ethidium bromide staining. Following excision from the gel, PCR products were cleaned up using the QIAquick Gel Purification Kit (Qiagen) according to the manufacturer's instructions and ligated into pDRIVE using the Qiagen PCR Cloning Kit (Qiagen). Plasmid DNA was isolated from individual clones, analysed by restriction enzyme digest and a number of positive clones were sequenced commercially (MWG Biotech, Milton Keynes, UK) and assembled using Sequencher (Genecodes, USA). *Et*ENR was expressed as a maltose binding protein (MBP) fusion protein using pMALLcHT vector (Muench et al., 2003) in BL21-Star (DE3) in the presence of pRIL, which encodes the tobacco etch virus (TEV) protease (Kapust and Waugh, 2000).

2.4. Antibodies

To generate antibodies to *Et*ENR, 50 μg of purified recombinant *Et*ENR protein was emulsified in FCA (Sigma) (1:1) and injected s.c. into BALB/c mice. On day 14, a secondary immunisation of 50 μg of recombinant *Et*ENR emulsified in Freund's incomplete adjuvant (Sigma) (1:1) was administered s.c. Blood was collected 14 days after the secondary immunisation. Serum samples were checked by Western blot analysis against purified recombinant *Et*ENR.

Additional antibodies used in the study were: anti-*Et*MIC2, which is a rabbit antibody to the microneme 2 protein of *E. tenella* (Tomley et al., 1996) and anti-*Et*SAG4 which stained the surface of the merozoites of *E. tenella* (Tabares et al., 2004).

2.5. Western blot analysis

Samples for analysis were mixed 1:1 with SDS–PAGE sample buffer (125 mM Tris, 4% SDS, 20% glycerol, 10% β-mercaptoethanol, 0.0025% bromophenol blue) and were boiled for 5 min before resolving on a 4% stacking/12% resolving SDS gel at 200 V constant voltage (Laemmli, 1970). The separated proteins were transferred to Hybond-ECL nitrocellulose membrane (Amersham Biosciences) using the Xcell Surelock system (Invitrogen) in Tris Glycine transfer buffer (50 mM Tris, 192 mM glycine, 20% methanol) for 1 h at 100 V constant voltage. After blotting, the membrane was blocked with 1% milk powder in PBS. Membranes were incubated for 1 h at room temperature with each mouse *Et*ENR antibody (1:10,000) and washed three times with PBS for 5 min. Membranes were then incubated with a horse anti-mouse IgG (Cell Signalling Technology) (1:3000) for 1 h, washed three times with PBS for 5 min, and developed using SuperSignal West Pico Chemiluminescent Substrate (Pierce).

2.6. Infection

Six week old Light Sussex chickens were infected by feeding sporulated oocysts of *E. tenella*. The infective dose was varied depending on the time to autopsy. Ten million oocysts were fed to chickens autopsied at 48 (first generation schizonts), 72 and 94 h, while 250,000 and 100,000 oocysts were used for chickens autopsied at 112 h (second generation schizonts) and 136 h (sexual stages) p.i., respectively.

2.7. Autopsy

The caecum of the chickens was removed and divided into two portions, one of which was fixed in 2% paraformaldehyde in 0.1 M phosphate buffer. Parts of this sample were dehydrated and embedded in wax for routine and immuno light microscopy. In addition, small portions were dehydrated and embedded in LR White resin for immunoelectron microscopy. The other portion was fixed in 4% glutaraldehyde in 0.1 M phosphate buffer and processed for routine EM as described previously (Ferguson et al., 1999). One micron sections of the plastic embedded material were also stained with azure A and examined by light microscopy to provide improved morphological detail and to identify areas of interest for EM.

2.8. Immunocytochemistry

Sections were pre-treated by pressure-cooking prior to immunostaining. Non-specific staining was blocked with 1% BSA in PBS. For immuno-peroxidase staining, serial sections from each time point were exposed to mouse anti-*Et*ENR, rabbit anti-*Et*MIC2 or chicken anti-*Et*SAG4. After washing, the sections were exposed to antibodies to the primary species immunoglobulins conjugated to peroxidase. DAB/H_2O_2 was used as the chromogen and the sections were counter-stained with haematoxylin prior to examination. For immunofluorescence staining, after pressure cooking and blocking, sections were single-labelled with anti-*Et*ENR or double-labelled with mouse anti-*Et*ENR and rabbit anti-*Et*MIC2, or chicken anti-*Et*SAG4 followed by anti-mouse Ig conjugated to fluorescein isothiocyanate (FITC) and anti-rabbit Ig or anti-chicken Ig conjugated to Texas red. Sections were counter stained with 4′,6-diamidino-2-phenylindole (DAPI) prior to examination.

In addition, smears of sporozoites obtained by excysting oocysts were fixed in paraformaldehyde and treated with acetone. Smears were stained with anti-*Et*ENR or for double labelling, mouse anti-*Et*ENR and rabbit anti-*Et*MIC2 followed by anti-mouse Ig conjugated to FITC or in combination with anti-rabbit Ig conjugated to Texas red. Smears were finally counter-stained with DAPI.

2.9. Electron microscopy and immunoelectron microscopy

For routine EM, thin sections were stained with uranyl acetate and lead citrate prior to examination in a Jeol 1200EX electron microscope. For immunoelectron microscopy, thin sections were place on formvar-coated nickel grids. The grids were floated on drops of 1% BSA in PBS to block non-specific staining and then on the primary antibody (*Et*ENR or *Et*MIC2) in PBS. After washing, the grids were exposed to secondary anti-primary Ig conjugated to 10 nm gold particles. Sections were counter-stained with uranyl acetate prior to examination.

2.10. Phylogenetic analyses of ENR gene

BLASTp and tBLASTn were used to sample similar homologues to *Et*ENR from the following genome project databases: GenBank nr database and the *Entamoeba histolytica*, *Dictyostelium discoideum*, *Giardia intestinalis*, *Trichomonas vaginalis*, *Leishmania major*, *Trypanosoma brucei*, *Trypanosoma cruzi*, *Plasmodium yoelii*, *P. falciparum*, *Tetrahymena thermophila*, *Phytophthora ramorum*, *Thalassiosira pseudonana*, *Ustilago maydis*, *Cryptococcus neoformans*, *Rhizopus oryzae*, *Neurospora crassa*, *Chlamydomonas reinhardtii*, *Arabidopsis thaliana*, *Homo sapiens*, *Drosophila melanogaster*, *Caenorhabditis elegans* and *Cyanidioschyzon merolae* genome databases. Sequence data was obtained from The Institute for Genomic Research website (http://www.tigr.org), Department of Energy Joint Genome Institute (http://www.jgi.doe.gov) and the *C. merolae* genome website (http://merolae.biol.s.u-tokyo.ac.jp/). In addition, a range of prokaryote putative homologues were sampled, attention was paid to include best scoring cyanobacteria and the α-proteobacterial sequences. Sequences were sampled when BLAST e-scores exceeded 4e-22 to focus the analyses on a putative set of orthologues or closely related paralogues. Sequences were aligned using T-COFFEE (Notredame et al., 2000) and manually refined using SE-AL (Rambaut, A., 1996. Se-Al:Sequence Alignment Editor. Available at http://evolve.zoo.ox.ac.uk/.). Ambiguous or highly variant alignment positions were excluded (masked) in preparation for phylogenetic analyses. The edited and masked alignment was then evaluated using the program MODELGENERATOR (Keane, T.M., 2004. MODELGENERATOR download [http://bioinf.nuim.ie/software/modelgenerator/].) to ascertain the best model for phylogeny (which compares the likelihood ratio score of a neighbour-joining tree) given the alignment using different models of amino acid substitution with different combinations of Γ and Pinvar corrections for site rate heterogeneity (WAG + Γ8 + I). Bayesian analysis was performed using MRBAYES 3.1.2 (Ronquist and Huelsenbeck, 2003) incorporating a rate variation across sites model with eight category gamma distribution and proportion of invariant sites. The MCMCMC was run twice independently, each with four chains (one cold, three heated) for 500,000 generations with a sampling frequency of every 100 generations. Parameters and likelihood values were plotted to confirm that the values had converged between the two analyses and reached a plateau by 50,000 generations (500 samples) allowing us to conservatively discard the first 500 samples as “burnin”. Maximum Likelihood bootstrap values from 1,000 replicates were generated using PHYML (Guindon and Gascuel, 2003; Guindon et al., 2005) using the same model as predicted by MODELGENERATOR.

2.11. Bioinformatics for division proteins

Sequences of proteins known to be involved in plastid division of *A. thaliana* were identified in the NCBI nr database (www.ncbi.nlm.nih.gov) and used as queries to search the *E. tenella* genome project database (http://www.sanger.ac.uk) using the tBLASTn algorithm. Those searched for were: MinD, Dynamin, Centrin, FtsZ and FtsK, MSCL proteins, ZipA and ArcII. The *Eimeria* homologous sequences found were translated in MacVector™ 7.0. The predicted open reading frames (ORFs) were aligned using CLUSTALW (Thompson et al., 1994).

3. Results

3.1. Identification of Type II fatty acid synthase enzymes

DNA sequences were identified that contained potential coding regions homologous to several enzymes of the FASII pathway (Type II β-ketoacyl-ACP synthase [β-KAS]. β-ketoacyl-ACP reductase [β-KAR], β-hydroxyacyl-ACP dehydrase [β-HAD] and enoyl-ACP reductase [ENR]) which show approximately, 30%, 40%, 30% and 40% sequence identity to their homologues in *P. falciparum*, respectively. Moreover, analysis of these sequences when aligned with their homologues from other species reveals that they all retain the residues which have been shown to be important for catalysis (Supplementary Fig. 1; Rafferty et al., 1995; Heath et al., 2001; Price et al., 2001, 2004; Swarnamukhi et al., 2006). Of the remaining two enzymes of the FASII pathway only partial sequence could be obtained containing 150 residues that aligned with the C-terminal section of the *P. falciparum* Type III β-KAS protein with approximately 50% sequence identity, whereas the sequence for malonyl-CoA-ACP transacylase [ACAT] is made up of several contigs. These results indicate that *E. tenella* like its apicomplexan counterparts *T. gondii* and *P. falciparum* can utilize a FASII pathway.

Further analysis focussed on the genomic contig 2257242.c009402138, as it contained potential coding sequences similar to those already described in known ENR proteins that are the target of the antimicrobial, triclosan. As the genomic sequence appeared to include multiple introns, a region flanking the predicted ENR ORF was amplified by PCR from *E. tenella* cDNA, cloned and sequenced. This revealed an ORF of 1233 bp encoding a protein of 411 amino acids with a predicted molecular weight of 42.8 kDa. Comparison of the cDNA with the gDNA reveals that the coding region is composed of five introns and six exons.

3.2. Analysis of EtENR

The amino acid sequence of *Et*ENR is highly conserved when compared with other ENR homologues with significant sequence similarity of 65%, 59% and 42% between the ENR enzyme from *T. gondii*, *Brassica napus* and *P. falciparum*, respectively, which suggests that it is a homologous protein with the potential to adopt a fold similar to that seen for other members of the ENR family. In common with previously described apicomplexan ENRs, *Et*ENR has a predicted bi-partite transit sequence consisting of a cleavable von Heijne secretory signal (amino acids 1–25) and a chloroplast-like transit sequence (amino acids 26–91) facilitating targeting and entry to the apicoplast (Fig. 1). A common feature of both plant and apicomplexan ENR sequences is the presence of two significant insertions, both before and after β3 [Arg58 to Ile71 and Leu79 to Asp103 (*Tg*ENR numbering) which form a groove on the top of the ENR tetramer, a feature absent in the bacterial ENR homologues (Muench et al., unpublished data). Furthermore, *Et*ENR also contains a hydrophilic insert after α7 common to the apicomplexan ENR family which flanks the substrate binding domain and can vary in length from 37 amino acids (*P. falciparum*) to six amino acids (*T. gondii*), with close sequence similarity for the later in *Et*ENR (Fig. 1). This sequence character, although highly variable, is present only in the chromalveolate sequences and so represents a character (synapomorphy) consistent with chromalveolate holophyly (Harper and Keeling, 2003) confirmed with 83% bootstrap support for monophyly of these taxa (Fig. 2). Phylogenetic analyses also demonstrates that the *Et*ENR gene is an orthologue of the previously studied *Toxoplasma* gene (Ferguson et al., 2005) and that the chromalveolate ENR genes branch with the Viridaeplantae and the Chlamydia genes consistent with an origin from the plastid progenitor genome (Brinkman et al., 2002). Several branching relationships were weakly supported, suggesting that these relationships are undefined. In addition, the relationships within the Apicomplexa did not conform to expected species relationships, with the *Plasmodium* species branching separately from the other apicomplexans. This unexpected branching relationship suggests the possibility of hidden paralogy within the chromalveolates or, alternatively, the presence of a

tree reconstruction artifact in the analyses. As such the results of the phylogenetic analyses are unlikely to represent a good model for chromalveolate evolutionary relationships. All the residues known to be involved in binding the antimicrobial triclosan, a potent inhibitor of ENR, are conserved between *Et*ENR and other apicomplexan homologues (Fig. 1a and b). Interestingly, of those residues that appeared to be conserved across all species, one exception is found within *Et*ENR in which Ala119 is replaced by a cysteine. This is not a PCR error as several different PCR products were sequenced from a number of independent reactions and this sequence also corresponds with the genomic sequence obtained from the database. A feature that is unique to *Et*ENR is that Cys 295 lies in close proximity to Cys312 with their separation being consistent with disulphide bond formation (Fig. 1c). Other than the potential of these amino acid substitutions to facilitate a disulphide bond formation, the full implications of this observation are yet to be realised. However, their positions on a6 and b6, (based on known structures), would place this change approximately 11 Å from the active site. Furthermore, this residue is buried within the core of the protein and makes interactions with less conserved residues and as such a replacement from alanine to cysteine would appear to have little effect if any on the *Et*ENR structure (Fig. 1b and c).

The antibodies generated against the recombinant *Et*ENR protein were tested against both recombinant protein and also an extract from second generation merozoites and were found to recognise a band of approximately 42.8 kDa in both cases (Supplementary Fig. 2).

3.3. Genome-to-genome comparisons of candidate apicoplast division machinery

BLAST searches identified contigs in *E. tenella* genomic database that contain ORFs with similarity to the plastid division machinery of *A. thaliana*, *C. merolae* and *C. reinhardtii*. Partial Dynamin and MinD sequences were identified as well as two Centrin sequences. FtsZ, FtsK, MSCL, ArcII and ZipA proteins were not found. The highest BLAST hits for *E. tenella* Dynamin, MinD and Centrin are other apicomplexans, ciliates, bacteria and metazoans (Table 1). These proteins are involved in the division of other organelles in various taxa and therefore cannot be definitely associated with apicoplast division without further experimental work.

3.4. Microscopy

3.4.1. Sporozoite—When sporozoites were examined by immunocytochemistry, a small *Et*ENR positive apicoplast was observed adjacent to the nucleus (Fig. 3a and b). Occasionally sporozoites (<5%) were observed with two or three apicoplasts, often on opposite sides of the nucleus (Fig. 3a). The *Et*ENR signal appeared to colocalise with a small DAPI positive structure consistent with the structure of the apicoplast (Fig. 3b–d).

3.4.2. Merozoite—All the mature first and second generation merozoites in the gut appeared to contain at least one small *Et*ENR positive apicoplast (Fig. 3f). However, based on counting 100 organisms, approximately 20% of merozoites had multiple apicoplasts with between two and four located around the nucleus, but predominantly posterior to the nucleus (Fig. 3e and f). These appearances correlated with the spherical multi-membrane apicoplasts identified by EM (Fig. 4a and b). In addition, immunoelectron microscopy confirmed that the *Et*ENR protein was located within these structures (Fig. 4c). The apicoplast was much smaller (approximately 400–450 nm in diameter) than the nucleus (approximately 1.3–1.5 μm diameter) and contained fine granular material (Fig. 4b).

3.4.3. Asexual development—*Eimeria tenella* undergoes a number of asexual cycles that have been identified as two generations based on differences of the timing, location and appearances of the schizonts (Fig. 3g and h). The second-generation schizonts of *E. tenella* were very large, produced a few hundred daughters and were located in epithelial cells within the mucosa of the caecum (Fig. 3h).

The structure and location of the apicoplast during asexual development were examined by immunocytochemistry using the peroxidase technique which allowed the host tissue architecture to be evaluated (Fig. 3g) or in double-labelled immunofluorescence in which antibodies to microneme proteins (*Et*MIC2) and surface proteins (*Et*SAG4) was used to identify merozoite formation (Figs. 3h and 5o, q). By examining a large number of images of parasites at various stages of development, it was possible to reconstruct the apparent sequence of events involved in schizogony. It was observed that the newly entered parasites contain one or more small apicoplast/s (Fig. 5a–c). In double-labelled sections, this early intracellular stage was characterised by the residual staining with microneme proteins such as *Et*MIC2 (Fig. 5c). Early development (one to eight nucleus stages) was associated with the loss of the microneme protein staining and a marked enlargement and increased staining intensity of the ENR positive apicoplast/s (Fig. 5d–f). The growth of the parasite was associated with repeated nuclear divisions and enlarged apicoplast/s, which were pleiomorphic in shape and reached a size of 1.5–2.0 μm in diameter (Fig. 5d–f). As this growth and nuclear division continued, the apicoplast also underwent division to form a number of apparently unconnected, well-separated large apicoplasts (Fig. 5g–i). This relationship continued with parasite growth and the apicoplasts were similar in size but fewer in number than the nuclei (Figs. 3g, h and 5h, i). Counting showed a ratio of approximately three nuclei to every large apicoplast.

When examined by EM, the early schizont contained a number of nuclei, resulting from repeated divisions, and a number of single or collections of vacuoles with homogenous contents of variable electron density (Fig. 4d). At higher magnification, these vacuoles were limited by multiple membranes. Four were consistently observed and appeared to characterise the apicoplast (Fig. 4e–h). By immunoelectron microscopy, the contents of these structures were uniformly labelled with anti-*Et*ENR confirming their identity as apicoplasts (not shown). At this stage, a number of lipid droplets were observed in the schizont cytoplasm (Fig. 4d).

From the immunocytochemistry and EM observations, the *Et*ENR positive structures (apicoplasts) had a complex morphology. Using light microscopy, many appeared to be crescentic or donut shaped (Fig. 5j) while using EM they appeared to consist of multiple vacuolar profiles (Fig. 4d and e). It is possible that these apparent individual *Et*ENR positive vacuoles represents a thin section through a single much-folded structure (Fig. 4f and g). Analysis of the substructural features of the apicoplasts identified localised areas of electron dense material forming plaques between the second and third membranes. This was a relatively common feature with approximately 25% of cross-sectioned apicoplasts displaying such plaques. In addition, under the inner membrane, longitudinal filaments were observed (Fig. 4h). It was also possible to find areas exhibiting constrictions or infolding of the inner membranes (Fig. 4i and j). Although the large apicoplasts were relatively close to the nuclei, there was no evidence of any direct association with the nuclear pole or centrioles. Often the apicoplasts were on the opposite side of the nucleus to the nuclear spindle (Fig. 6a).

Schizogony continued with the growth of the parasite and increasing numbers of nuclei and large apicoplasts with both organelles being randomly distributed throughout the cytoplasm (Figs. 3h and 5m). As the schizont increase in size, the surface area was further increase by deep invaginations of the plasmalemma (Fig. 5l).

Towards the end of the growth phase, but prior to the initiation of daughter formation, there appeared to be an unwinding of the large apicoplast into a thin elongated structure (Fig. 5j and m). These structures developed a bead-like appearance with numerous regular constrictions along its length and appeared to result in the formation of numerous small *Et*ENR positive apicoplasts (Fig. 5k and n). The small spherical *Et*ENR positive structures were similar in size (approximately 0.45 μm diameter) to the apicoplasts of the sporozoites and merozoite. The small apicoplasts were present in greater numbers (approximately 3:1) than the nuclei and were

randomly distributed throughout the cytoplasm (Fig. 3g and h). This final apicoplast division occurred before daughter formation was initiated as confirmed by the limited *Et*SAG4 staining and the absence of *Et*MIC2 staining (Figs. 3h and 5n).

The differentiation phase, resulting in merozoite formation, was associated with the nuclei and apicoplasts moving close to the schizont plasmalemma or its deep invaginations (Fig. 3h). The earliest stage of daughter formation was identified by increased expression of the anti-*Et*SAG4 at the schizont surface (Fig. 5o). At this stage, daughter formation was initiated by the formation of the conoid and inner membrane complex beneath the plasmalemma as observed by EM (Fig. 6b and c). The small *Et*ENR positive apicoplasts were predominately located on the cytoplasmic side of the nuclei (Figs. 3h and 5o). The merozoites were formed by budding into the parasitophorous vacuole while the inner membrane complex remaining anchored to the junction with the plasmalemma (Fig. 6c–f). The nuclear poles were directed into the forming daughters as the nucleus entered. As this process occurred, one or more apicoplasts also entered the developing merozoite. At this time, the micronemes formed in the anterior of the daughters as shown by positive staining for *Et*MIC2 (Figs. 3h and 5o). In the fully formed merozoite, between one and four small apicoplasts were located around the nucleus in each daughter (Fig. 5p and q). The segregation process during the differentiation phase resulted in a single nucleus and one to four apicoplasts entering every daughter with none left in the residual body.

3.4.4. Sexual stages

Microgametocyte development: The microgametocytes developed in the superficial epithelial cells of the crypts. In the heavily infected caecum, micro- and macrogametocytes developed in adjacent or even the same cell (Fig. 7a–c). The early stages were characterised by the presence of a numbers of open nuclei. At this time, one or more small apicoplasts with a relatively low *Et*ENR signal were located in the cytoplasm (Fig. 7b, c, e, f and i). During maturation the number of nuclei increased and became peripherally located with increasingly condensed chromatin (Fig. 7b and c). During this time, little change was seen in the apicoplast (Fig. 7b and c). In mature microgametocytes, the residual cytoplasm exhibited little evidence of apicoplasts and apicoplasts were not observed in the crescentic shaped microgametes formed (Fig. 7b and c)

Macrogametocyte development: In contrast to the microgametocytes, there was strong anti-*Et*ENR staining of enlarged lobated apicoplast/s located adjacent to the large single nucleus during the early stages of development (Fig. 7b–i). Due to the absence of suitable antibodies for staining other organelles of the macrogametocytes, the appearance of the apicoplast within the developing macrogamete is best seen using the peroxidase technique (Fig. 7b, e, g and h). Consistent with the lobed appearance of the apicoplast by immunofluorescence, multiple profiles of apicoplast-like structures adjacent to the nucleus were observed by EM (Fig. 8a and b) and confirmed by immunoelectron microscopy (Fig. 8c). The strongly staining apicoplast was maintained during the growth and maturation of the macrogametocyte with the development of the various types of wall forming bodies, polysaccharide granules and lipid droplets (Fig. 7f and g). Large or multiple *Et*ENR positive apicoplasts were still present within developing oocysts identified by the formation of the oocyst wall (Fig. 7h). Therefore, in the absence of apicoplasts associated with the microgamete, oocysts only inherited this organelle from the macrogametes, which is consistent with maternal inheritance by the sporozoites.

4. Discussion

Previous studies have identified enzymes of type II fatty acid synthesis in a number of apicomplexans including *T. gondii* and *Plasmodium* spp., but these are notably absent from *Cryptosporidium parvum* and *Cryptosporidium hominis* that lack apicoplasts (Abrahamsen et

al., 2004; Xu et al., 2004). Moreover, the type II fatty acid biosynthesis has been suggested as an antimicrobial agent target in *T. gondii* and *Plasmodium* spp. and as such the identification of the enzymes of type II fatty acid biosynthesis in *E. tenella* may suggest that this pathway holds promise as an antimicrobial target. Analysis of these genes reveals that they all show significant sequence similarity to their bacterial and apicomplexan homologues, in particular those residues which have been implicated in catalysis are all fully conserved in the *E. tenella* enzymes. This analysis may suggest that *E. tenella* contains a fully functioning type II fatty acid biosynthesis pathway. Of the seven enzymes involved in Type II fatty acid synthesis evident in the genome of *E. tenella*, we elected to further characterise ENR. This is because the structure of a number of ENRs has been solved both independently and in complex with several families of antimicrobial compounds including the diazaborines, aminopyridine-based inhibitors and triclosan (Baldock et al., 1996; Levy et al., 1999; Payne et al., 2002; Seefeld et al., 2003). Modelling of *Et*ENR based on the close homologue *T. gondii* ENR has revealed that those residues which form close interactions to the biocide triclosan are fully conserved in *Et*ENR and that features unique to the plastid but absent in the bacterial ENR family are conserved, including two significant sequence inserts before and after β3, common to the chromalveolate ENR orthologue (Fig. 1). Moreover, Cys295 is positioned in close proximity to Cys312 with their separation being consistent with disulphide bond formation a possibility that will require further investigation (Fig. 1c).

Expression of the predicted mature protein also facilitated the production of polyclonal antisera. These sera not only allowed confirmation of the apicoplast location of the enzyme, but also made it possible to visualise detailed changes in the morphology of the apicoplast throughout the life cycle of *E. tenella*. The present study involved the use of tissue samples from infected chickens. This is the only method available for examining many of the natural developmental processes involved in the coccidian lifecycle because these cannot be reproduced in tissue culture. This is particularly true for the coccidian stages of development (asexual and sexual) present in the definitive hosts. Unfortunately, there are a number of disadvantages of having to examine sections of fixed and embedded tissue. It is not possible to follow dynamic developmental processes within a given parasite. Second, the parasites are randomly orientated within the tissue increasing the difficulty of obtaining clear images, in contrast to the situation in cultured cells where the parasites are constrained to a flattened two-dimensional orientation. Third, many of the antibodies and fluorescent stains, which have added greatly to our knowledge of in vitro development, will not work with formalin fixed/wax embedded tissue. For example, in tissue sections, DAPI stain is insensitive and cannot be used to identify the apicoplast within the gut stages, probably due to extraction of material or a change in architecture during processing. The absence of DAPI staining of the macrogametocyte/macrogamete nucleus is unexpected, but similar to that reported for the macrogamete of *T. gondii* and is thought to relate the dispersed nature of the chromatin (Ferguson et al., 2005). However, careful examination of large numbers of immunostained parasites, correlated with detailed routine and immunoelectron microscopy can ameliorate these limitations.

The changes observed during sexual development are similar to those reported previously for *T. gondii* (Ferguson et al., 2005). The development of the microgametocyte results in little change to the apicoplast size, shape or staining intensity and the microgametes formed lacked an identifiable apicoplast. In the case of macrogametocyte development, there is a marked increase in size and staining intensity from the early stages up to and including the mature macrogamete and early oocyst. Unlike the schizont, there was no evident apicoplast division or reduced ENR signal in the mature macrogamete. This would point to a continued physiological function of the apicoplasts throughout macrogamete maturation. This may be reflected in the build up of storage lipid and polysaccharide granules within the cytoplasm. The apparent absence of the apicoplast in microgametes suggests that the apicoplast is inherited

from the macrogamete and is thus maternally derived as previously described for *T. gondii* and *Plasmodium* spp. (Ferguson et al., 2005; Vaidya et al., 1993; Creasey et al., 1994). Maternal inheritance of the plastid thus might be a common feature of the Apicomplexa.

In the infectious stages, the apicoplast is a small spherical structure with a relatively low *Et*ENR signal after immunostaining. While the physiological processes undertaken by the apicoplast are still incompletely understood, it is likely that the size of the apicoplast and level of *Et*ENR signal reflect changes in the activity of the apicoplast and type II fatty acid synthesis. Using the immunofluorescence technique, it is impossible to absolutely quantify *Et*ENR levels. However, differences in the size and signal intensity between identically stained parasites will represent quantitative changes in the relative concentrations of the protein. Using this criterion, it is obvious that one of the early changes during schizogony and macrogametogony is a marked increase in the size of the apicoplast and the level of *Et*ENR signal, which is not observed during microgametogony. Therefore, it is interesting to note that the stages showing an apparent increase in the *Et*ENR protein are also the stages (early schizont and macrogametocyte) when lipid droplets have been identified by EM. This increase in size and *Et*ENR signal is similar to that reported during endopolygeny in *T. gondii* (Ferguson et al., 2005).

The apicoplast within the infectious stage of *E. tenella* appears as single or multiple peri-nuclear spherical structures. Careful examination of merozoites by immunocytochemistry and electron microscopy confirm that these were individual apicoplasts and not profiles of an elongated structure. The presence of multiple apicoplasts in the merozoites has not been reported for the infectious stages of other members of the Apicomplexa. This was relatively uncommon in sporozoites (less than 5%), but more common in second generation merozoites (approximately 20%). Although the organelle is limited by four membranes there are areas where the membranes are difficult to resolve. This is similar to that described for *T. gondii*, *P. falciparum* and *Sarcocystis* sp. (Sheffield and Melton, 1968; Vivier and Petitprez, 1972; McFadden and Roos, 1999; Tomova et al., 2006) although three membranes have also been reported for *P. falciparum* (Hopkins et al., 1999). In the present study, no evidence was found to support the proposal that there are two membranes with the multi-membraned appearance resulting from extensive folding of the inner membrane (Kohler, 2005). A unique observation in *E. tenella* was the appearance of electron dense plaques of material between the second and third membranes (Fig. 4f and g) but the role of this material is unknown.

In the present study, of the large schizonts of *E. tenella*, there was evidence for some division of the large apicoplasts during the proliferative phase. This has not been observed previously in the smaller schizonts of *T. gondii* and *P. falciparum* (Waller et al., 2000; Ferguson et al., 2005; van Dooren et al., 2005) and probably relates to the very large size of the second generation schizonts. The finding of merozoites with multiple apicoplasts has not been observed before. In *P. falciparum*, it has been proposed that apicoplast division was delayed until after nuclear division by an unknown feedback mechanism to determine how many portions the apicoplast would be required to divide into (Waller et al., 2000). It is possible, that in the large complex schizonts of *E. tenella* with hundreds of nuclei, such a feedback mechanism may not function and therefore the production of an excess number of apicoplasts may represent insurance against a shortage of apicoplasts. It is known that merozoites lacking an apicoplast are non-viable (He et al., 2001). Therefore, if there is no detrimental effect of having more than one apicoplast, then too many is better than too few.

The division mechanism of the apicoplast during asexual development within the Apicomplexa has been the subject of much controversy. Plastid division had been extensively studied in other systems and a range of proteins identified that play vital roles during bacterial cell division and the division of plastids (chloroplasts) in algae and plants (reviewed by Hashimoto, 2003). However, searches of the genomic data bases of apicomplexan parasites, in particular *P.*

falciparum, *T. gondii* and *E. tenella* (Vaishnava and Striepen, 2006; present study) have failed to identify a complete set of homologous genes for the plastid division proteins. Therefore a new mechanism had to be considered and two hypotheses are proposed from studies of endodyogeny in *T. gondii*. One involved a physical pull/push mechanism in which the centrioles/nuclear poles of the nuclear spindle are connected to and pull the apicoplast into an elongated structure as they move apart during nuclear division with the subsequent posterior growth of the inner membrane complex of the developing daughters pushing on the apicoplast to cause division (Striepen et al., 2000). The second hypothesis proposed that, even in the apparent absence of plastid division proteins, an unknown mechanism involving division/constriction rings may be involved in apicoplast division (Matsuzaki et al., 2001).

However, when comparing the results for apicoplast division and segregation within the Apicomplexa, it is important to realise that asexual multiplication is not a single process, but that there are subtle differences in the timing and location of both nuclear division and daughter formation undergone by different species and even between lifecycle stages of the same species. These differences may be relevant to understanding apicoplast division. We would propose that there are four distinct processes rather than the three suggested in a recent review (Vaishnava and Striepen, 2006). These we have termed "classical" schizogony, endodyogeny, "*Toxoplasma*" endopolygeny and "*Sarcocystis*" endopolygeny, with the distinctive and characteristic features being summarised in Fig. 9. The term endopolygeny has been used to describe asexual division involving internal formation of multiple daughters in both *T. gondii* and *Sarcocystis* sp. (Piekarski et al., 1971; Speer and Dubey, 2001). However, there are significant differences in relation to the presence or absence of repeated nuclear divisions in these processes (Fig. 9). Therefore we distinguish between the processes by using the terms "*Toxoplasma*" endopolygeny where there are repeated nuclear divisions and "*Sarcocystis*" endopolygeny where there are repeated DNA replications but no nuclear division (Fig. 9).

There is support for the pull/push hypothesis from studies of endodyogeny and "*Sarcocystis*" endopolygeny (Striepen et al., 2000; Vaishnava et al., 2005; Vaishnava and Striepen, 2006). However, it is difficult to reconcile apicoplast division directly to nuclear division and daughter formation in "*Toxoplasma*" endopolygeny and "classical" schizogony (Ferguson et al., 2005; Waller et al., 2002; present study) where repeated nuclear divisions occur in the absence of apicoplast division and apicoplast division occurs prior to daughter formation. In endodyogeny and "*Sarcocystis*" endopolygeny, although the processes of nuclear division, apicoplast division and initiation of daughter formation appear to be closely associated, they could still represent independent events.

In support of a constriction ring hypothesis is the observation of repeated constrictions along the large apicoplast in the absence of any association with nuclear division or daughter formation in "classical" schizogony and "*Toxoplasma*" endopolygeny. Indeed our search of the *E. tenella* genome has identified a number of genes for proteins that are believed to be associated with organellar division such as dynamin and MinD. However, there is no evidence that these are directly involved in apicoplast division and the very high similarity of the putative *E. tenella* MinD with a homologous protein in *C. parvum*, which lacks an identifiable apicoplast, suggests an alternative function for this molecule. Therefore, at the present time, the mechanism of apicoplast division remains an open question.

It should be noted that it is unclear how any of the genome containing organelles of the Apicomplexa (nucleus, mitochondrion and apicoplast) divide while maintaining intact membranes. It has recently been reported that division of the Golgi body during endodyogeny in *T. gondii* involved elongation of the stack of flattened vacuoles forming the organelle followed by division in the central region to form two organelles (Pelletier et al., 2002). Unfortunately, no mechanism was provided for how this elongation and central division of the

membranes occurs but it bears certain similarities to apicoplast elongation seen during endodyogeny.

However, irrespective of the involvement of the centrioles/nuclear pole in apicoplast division, they appear to play a central role in coordinating and organising daughter formation and organelle segregation. In the present study, just prior to the initiation of daughter formation, there is a redistribution of the organelles with the randomly distributed nuclei and apicoplasts moving to the periphery of the schizont close to the plasmalemma. In this situation, the centrioles/nuclear pole complex is pointed towards the plasmalemma and may direct the initiation of daughter formation thus ensuring the number of daughters matches the number of nuclei. The reestablishment of the nucleus and apicoplast relationship and the movement of the centrioles/nuclear pole into the developing daughter will also ensure correct organelle segregation. The involvement of the centriolar complex during segregation, but not division, of the plastid would be consistent with that reported in certain brown alga that also acquired their plastid apparatus from a secondary endosymbiotic event (Nagasato and Motomura, 2002). Therefore the centrioles/nuclear pole may act as a coordinating centre ensuring efficient formation of viable daughters in all variations of the asexual proliferation process undergone by the Apicomplexa (Waller et al., 2000; Striepen et al., 2000; Ferguson et al., 2005; Vaishnava et al., 2005)

In conclusion, we propose a unifying theory for the nature of apicoplast development, which would be consistent with the observations across the Apicomplexa (Striepen et al., 2000; Waller et al., 2000; Ferguson et al., 2005; Vaishnava et al., 2005): (i) Nuclear and apicoplast division are independent events. (ii) Apicoplast division is independent of daughter formation and could involve constriction rings of unknown composition. (iii) The centriolar/nuclear complex appears to play a central role in coordinating daughter formation and organelle segregation. It is possible that, an as yet to be discovered, unifying mechanism may explain how the Golgi body, nucleus, apicoplast and mitochondrion divide while retaining intact membranes. A better understanding of how these processes are controlled and coordinated would be a major advance in our understanding of the Apicomplexa.

Supplementary Material

Refer to Web version on PubMed Central for supplementary material.

Acknowledgments

This work was supported by NIH grants R01 AI43228 (R.M. and C.W.R.) and AI27530 (R.M.), the Research to Prevent Blindness Foundation (R.M.) and a Wellcome Trust equipment grant (D.J.P.F). Ms. H. Beard is thanked for assistance in preparing the diagram in Fig. 9.

References

Abrahamsen MS, Templeton TJ, Enomoto S, Abrahante JE, Zhu G, Lancto CA, Deng M, Liu C, Widmer G, Tzipori S, Buck GA, Xu P, Bankier AT, Dear PH, Konfortov BA, Spriggs HF, Iyer L, Anantharaman V, Aravind L, Kapur V. Complete genome sequence of the apicomplexan, *Cryptosporidium parvum*. Science 2004;304:441–445. [PubMed: 15044751]

Baldock C, Rafferty JB, Sedelnikova SE, Baker PJ, Stuitje AR, Slabas AR, Hawkes TR, Rice DW. A mechanism of drug action revealed by structural studies of enoyl reductase. Science 1996;274:2107–2110. [PubMed: 8953047]

Brinkman FS, Blanchard JL, Cherkasov A, Av-Gay Y, Brunham RC, Fernandez RC, Finlay BB, Otto SP, Ouellette BF, Keeling PJ, Rose AM, Hancock RE, Jones SJ, Greberg H. Evidence that plant-like genes in Chlamydia species reflect an ancestral relationship between Chlamydiaceae, cyanobacteria, and the chloroplast. Genome Res 2002;12:1159–1167. [PubMed: 12176923]

Cai X, Fuller AL, McDougald LR, Zhu G. Apicoplast genome of the coccidian *Eimeria tenella*. Gene 2003;321:39–46. [PubMed: 14636990]

Cavalier-Smith T. Membrane heredity and early chloroplast evolution. Trends Plant Sci 2000;5:174–182. [PubMed: 10740299]

Creasey A, Mendis K, Carlton J, Williamson D, Wilson I, Carter R. Maternal inheritance of extrachromosomal DNA in malaria parasites. Mol Biochem Parasitol 1994;65:95–98. [PubMed: 7935632]

Fast NM, Xue L, Bingham S, Keeling PJ. Re-examining alveolate evolution using multiple protein molecular phylogenies. J Eukaryot Microbiol 2002;49:30–37. [PubMed: 11908896]

Ferguson DJ. *Toxoplasma gondii* and sex: essential or optional extra? Trends Parasitol 2002;18:355–359. [PubMed: 12380023]

Ferguson DJ, Birch-Andersen A, Hutchison WM, Siim JC. Ultrastructural studies on the endogenous development of *Eimeria brunetti*, I. Schizogony. Acta Pathol Microbiol Scand B 1976;84:401–413. [PubMed: 998258]

Ferguson DJ, Cesbron-Delauw MF, Dubremetz JF, Sibley LD, Joiner KA, Wright S. The expression and distribution of dense granule proteins in the enteric (Coccidian) forms of *Toxoplasma gondii* in the small intestine of the cat. Exp Parasitol 1999;91:203–211. [PubMed: 10072322]

Ferguson DJ, Henriquez FL, Kirisits MJ, Muench SP, Prigge ST, Rice DW, Roberts CW, McLeod RL. Maternal inheritance and stage-specific variation of the apicoplast in *Toxoplasma gondii* during development in the intermediate and definitive host. Eukaryot Cell 2005;4:814–826. [PubMed: 15821140]

Guindon S, Gascuel O. A simple, fast, and accurate algorithm to estimate large phylogenies by maximum likelihood. Syst Biol 2003;52:696–704. [PubMed: 14530136]

Guindon S, Lethiec F, Duroux P, Gascuel O. PHYML Online – a web server for fast maximum likelihood-based phylogenetic inference. Nucl Acids Res 2005;33:W557–W559. [PubMed: 15980534]

Harper JT, Keeling PJ. Nucleus-encoded, plastid-targeted glyceraldehyde-3-phosphate dehydrogenase (GAPDH) indicates a single origin of chromalveolate plastids. Mol Biol Evol 2003;20:1730–1735. [PubMed: 12885964]

Hashimoto H. Plastid division: its origins and evolution. Int Rev Cytol 2003;222:63–98. [PubMed: 12503847]

He CY, Shaw MK, Pletcher CH, Striepen B, Tilney LG, Roos DS. A plastid segregation defect in the protozoan parasite *Toxoplasma gondii*. EMBO J 2001;20:330–339. [PubMed: 11157740]

Heath RJ, White SW, Rock CO. Lipid biosynthesis as a target for antibacterial agents. Prog Lipid Res 2001;40:467–497. [PubMed: 11591436]

Hopkins J, Fowler R, Krishna S, Wilson I, Mitchell G, Bannister L. The plastid in *Plasmodium falciparum* asexual blood stages: a three-dimensional ultrastructural analysis. Protist 1999;150:283–295. [PubMed: 10575701]

Kapust RB, Waugh DS. Controlled intracellular processing of fusion proteins by TEV protease. Protein Expr Purif 2000;19:312–318. [PubMed: 10873547]

Kohler S. Multi-membrane-bound structures of Apicomplexa: I. the architecture of the *Toxoplasma gondii* apicoplast. Parasitol Res 2005;96:258–272. [PubMed: 15895255]

Kohler S, Delwiche CF, Denny PW, Tilney LG, Webster P, Wilson RJ, Palmer JD, Roos DS. A plastid of probable green algal origin in Apicomplexan parasites. Science 1997;275:1485–1489. [PubMed: 9045615]

Laemmli UK. Cleavage of structural proteins during the assembly of the head of bacteriophage T4. Nature 1970;227:680–685. [PubMed: 5432063]

Levine ND, Corliss JO, Cox FE, Deroux G, Grain J, Honigberg BM, Leedale GF, Loeblich AR Jr, Lom J, Lynn D, Merinfeld EG, Page FC, Poljansky G, Sprague V, Vavra J, Wallace FG. A newly revised classification of the protozoa. J Protozool 1980;27:37–58. [PubMed: 6989987]

Levy CW, Roujeinikova A, Sedelnikova S, Baker PJ, Stuitje AR, Slabas AR, Rice DW, Rafferty JB. Molecular basis of triclosan activity. Nature 1999;398:383–384. [PubMed: 10201369]

Matsuzaki M, Kikuchi T, Kita K, Kojima S, Kuroiwa T. Large amounts of apicoplast nucleoid DNA and its segregation in *Toxoplasma gondii*. Protoplasma 2001;218:180–191. [PubMed: 11770434]

McFadden GI, Roos DS. Apicomplexan plastids as drug targets. Trends Microbiol 1999;7:328–333. [PubMed: 10431206]

McFadden GI, Waller RF. Plastids in parasites of humans. Bioessays 1997;19:1033–1040. [PubMed: 9394626]

McLeod R, Muench SP, Rafferty JB, Kyle DE, Mui EJ, Kirisits MJ, Mack DG, Roberts CW, Samuel BU, Lyons RE, Dorris M, Milhous WK, Rice DW. Triclosan inhibits the growth of *Plasmodium falciparum* and *Toxoplasma gondii* by inhibition of apicomplexan Fab I. Int. J Parasitol 2001;31:109–113.

Muench SP, Rafferty JB, McLeod RL, Rice DW, Prigge ST. Expression, purification and crystallization of the *Plasmodium falciparum* enoyl reductase. Acta Crystallogr D Biol Crystallogr 2003;59:1246–1248. [PubMed: 12832774]

Nagasato C, Motomura T. Influence of the centrosome in cytokinesis of brown algae: polyspermic zygotes of *Scytosiphon lomentaria* (Scytosiphonales, Phaeophyceae). J Cell Sci 2002;115:2541–2548. [PubMed: 12045224]

Notredame C, Higgins DG, Heringa J. T-Coffee: A novel method for fast and accurate multiple sequence alignment. J Mol Biol 2000;302:205–217. [PubMed: 10964570]

Payne DJ, Miller WH, Berry V, Brosky J, Burgess WJ, Chen E, DeWolf WE Jr, Fosberry AP, Greenwood R, Head MS, Heerding DA, Janson CA, Jaworski DD, Keller PM, Manley PJ, Moore TD, Newlander KA, Pearson S, Polizzi BJ, Qiu X, Rittenhouse SF, Slater-Radosti C, Salyers KL, Seefeld MA, Smyth MG, Takata DT, Uzinskas IN, Vaidya K, Wallis NG, Winram SB, Yuan CC, Huffman WF. Discovery of a novel and potent class of FabI-directed antibacterial agents. Antimicrob Agents Chemother 2002;46:3118–3124. [PubMed: 12234833]

Pelletier L, Stern CA, Pypaert M, She D, Ngo HM, Roper N, He CY, Hu K, Toomre D, Coppens I, Roos DS, Joiner KA, Warren G. Golgi biogenesis in *Toxoplasma gondii*. Nature 2002;418:548–552. [PubMed: 12152082]

Piekarski G, Pelster B, Witte HM. Endopolygenie bei in *Toxoplasma gondii*. Z Parasitenkd 1971;36:122–130. [PubMed: 5555447]

Price AC, Choi KH, Heath RJ, Li Z, White SW, Rock CO. Inhibition of beta-ketoacyl-acyl carrier protein synthases by thiolactomycin and cerulenin. Structure and mechanism. J Biol Chem 2001;276:6551–6559. [PubMed: 11050088]

Price AC, Zhang YM, Rock CO, White SW. Cofactor-induced conformational rearrangements establish a catalytically competent active site and a proton relay conduit in FabG. Structure 2004;12:417–428. [PubMed: 15016358]

Rafferty JB, Simon JW, Baldock C, Artymiuk PJ, Baker PJ, Stuitje AR, Slabas AR, Rice DW. Common themes in redox chemistry emerge from the X-ray structure of oilseed rape (*Brassica napus*) enoyl acyl carrier protein reductase. Structure 1995;3:927–938. [PubMed: 8535786]

Ralph SA, van Dooren GG, Waller RF, Crawford MJ, Martin JM, Foth BJ, Tonkin CJ, Roos DS, McFadden GI. Metabolic maps and functions of the *Plasmodium falciparum* apicoplast. Nat Rev Microbiol 2004;2:203–216. [PubMed: 15083156]

Roberts CW, McLeod R, Rice DW, Ginger M, Chance ML, Goad LJ. Fatty acid and sterol metabolism: potential antimicrobial targets in apicomplexan and trypanosomatid parasitic protozoa. Mol Biochem Parasitol 2003;126:129–142. [PubMed: 12615312]

Ronquist F, Huelsenbeck JP. MrBayes 3: Bayesian phylogenetic inference under mixed models. Bioinformatics 2003;19:1572–1574. [PubMed: 12912839]

Seefeld MA, Miller WH, Newlander KA, Burgess WJ, DeWolf WE Jr, Elkins PA, Head MS, Jakas DR, Janson CA, Keller PM, Manley PJ, Moore TD, Payne DJ, Pearson S, Polizzi BJ, Qiu X, Rittenhouse SF, Uzinskas IN, Wallis NG, Huffman WF. Indole naphthyridinones as inhibitors of bacterial enoyl-ACP reductases FabI and FabK. J Med Chem 2003;46:1627–1635. [PubMed: 12699381]

Sheffield HG, Melton ML. The fine structure and reproduction of *Toxoplasma gondii*. J Parasitol 1968;54:209–226. [PubMed: 5647101]

Snow RW, Guerra CA, Noor AM, Myint HY, Hay SI. The global distribution of clinical episodes of *Plasmodium falciparum* malaria. Nature 2005;434:214–217. [PubMed: 15759000]

Speer CA, Dubey JP. Ultrastructure of schizonts and merozoites of *Sarcocystis neurona*. Vet Parasitol 2001;95:263–271. [PubMed: 11223206]

Striepen B, Crawford MJ, Shaw MK, Tilney LG, Seeber F, Roos DS. The plastid of *Toxoplasma gondii* is divided by association with the centrosomes. J Cell Biol 2000;151:1423–1434. [PubMed: 11134072]

Surolia N, Surolia A. Triclosan offers protection against blood stages of malaria by inhibiting enoyl-ACP reductase of *Plasmodium falciparum*. Nat Med 2001;7:167–173. [PubMed: 11175846]

Swarnamukhi PL, Sharma SK, Bajaj P, Surolia N, Surolia A, Suguna K. Crystal structure of dimeric FabZ of *Plasmodium falciparum* reveals conformational switching to active hexamers by peptide flips. FEBS Lett 2006;580:2653–2660. [PubMed: 16643907]

Tabares E, Ferguson D, Clark J, Soon PE, Wan KL, Tomley F. *Eimeria tenella* sporozoites and merozoites differentially express glycosylphosphatidylinositol-anchored variant surface proteins. Mol Biochem Parasitol 2004;135:123–132. [PubMed: 15287593]

Tomova C, Geerts WJ, Muller-Reichert T, Entzeroth R, Humbel BM. New comprehension of the apicoplast of *Sarcocystis* by transmission electron tomography. Biol Cell 2006;98:535–545. [PubMed: 16706752]

Thompson JD, Higgins DG, Gibson TJ. CLUSTAL W: improving the sensitivity of progressive multiple sequence alignment through sequence weighting, position-specific gap penalties and weight matrix choice. Nucl Acids Res 1994;22:4673–4680. [PubMed: 7984417]

Tomley FM, Bumstead JM, Billington KJ, Dunn PP. Molecular cloning and characterization of a novel acidic microneme protein (Etmic-2) from the apicomplexan protozoan parasite, *Eimeria tenella*. Mol Biochem Parasitol 1996;79:195–206. [PubMed: 8855556]

Vaidya AB, Morrisey J, Plowe CV, Kaslow DC, Wellems TE. Unidirectional dominance of cytoplasmic inheritance in two genetic crosses of *Plasmodium falciparum*. Mol Cell Biol 1993;13:7349–7357. [PubMed: 8246955]

Vaishnava S, Striepen B. The cell biology of secondary endosymbiosis – how parasites build, divide and segregate the apicoplast. Mol Microbiol 2006;61:1380–1387. [PubMed: 16968220]

Vaishnava S, Morrison DP, Gaji RY, Murray JM, Entzeroth R, Howe DK, Striepen B. Plastid segregation and cell division in the apicomplexan parasite *Sarcocystis neurona*. J Cell Sci 2005;118:3397–3407. [PubMed: 16079283]

van Dooren GG, Marti M, Tonkin CJ, Stimmler LM, Cowman AF, McFadden GI. Development of the endoplasmic reticulum, mitochondrion and apicoplast during the asexual life cycle of *Plasmodium falciparum*. Mol Microbiol 2005;57:405–419. [PubMed: 15978074]

Vivier E, Petitprez A. Donnees ultrastructurales complementaires morphologiques et cytochemiques, sur *Toxoplasma gondii*. Protistologica 1972;8:199–221.

Wallach M. The development of CoxAbic® a novel vaccine against coccidiosis. World Poultry 2002;18:2–4.

Waller RF, McFadden GI. The apicoplast: a review of the derived plastid of apicomplexan parasites. Curr Issues Mol Biol 2005;7:57–79. [PubMed: 15580780]

Waller RF, Keeling PJ, Donald RG, Striepen B, Handman E, Lang-Unnasch N, Cowman AF, Besra GS, Roos DS, McFadden GI. Nuclear-encoded proteins target to the plastid in *Toxoplasma gondii* and *Plasmodium falciparum*. Proc Natl Acad Sci USA 1998;95:12352–12357. [PubMed: 9770490]

Waller RF, Reed MB, Cowman AF, McFadden GI. Protein trafficking to the plastid of *Plasmodium falciparum* is via the secretory pathway. EMBO J 2000;19:1794–1802. [PubMed: 10775264]

Wilson RJ. Progress with parasite plastids. J Mol Biol 2002;319:257–274. [PubMed: 12051904]

Xu P, Widmer G, Wang Y, Ozaki LS, Alves JM, Serrano MG, Puiu D, Manque P, Akiyoshi D, Mackey AJ, Pearson WR, Dear PH, Bankier AT, Peterson DL, Abrahamsen MS, Kapur V, Tzipori S, Buck GA. The genome of *Cryptosporidium hominis*. Nature 2004;431:1107–1112. [PubMed: 15510150]

Zuther E, Johnson JJ, Haselkorn R, McLeod R, Gornicki P. Growth of *Toxoplasma gondii* is inhibited by aryloxyphenoxypropionate herbicides targeting acetyl-CoA carboxylase. Proc Natl Acad Sci USA 1999;96:13387–13392. [PubMed: 10557330]

Appendix A. Supplementary data

Supplementary data associated with this article can be found, in the online version, at doi: 10.1016/j.ijpara. 2006.10.003.

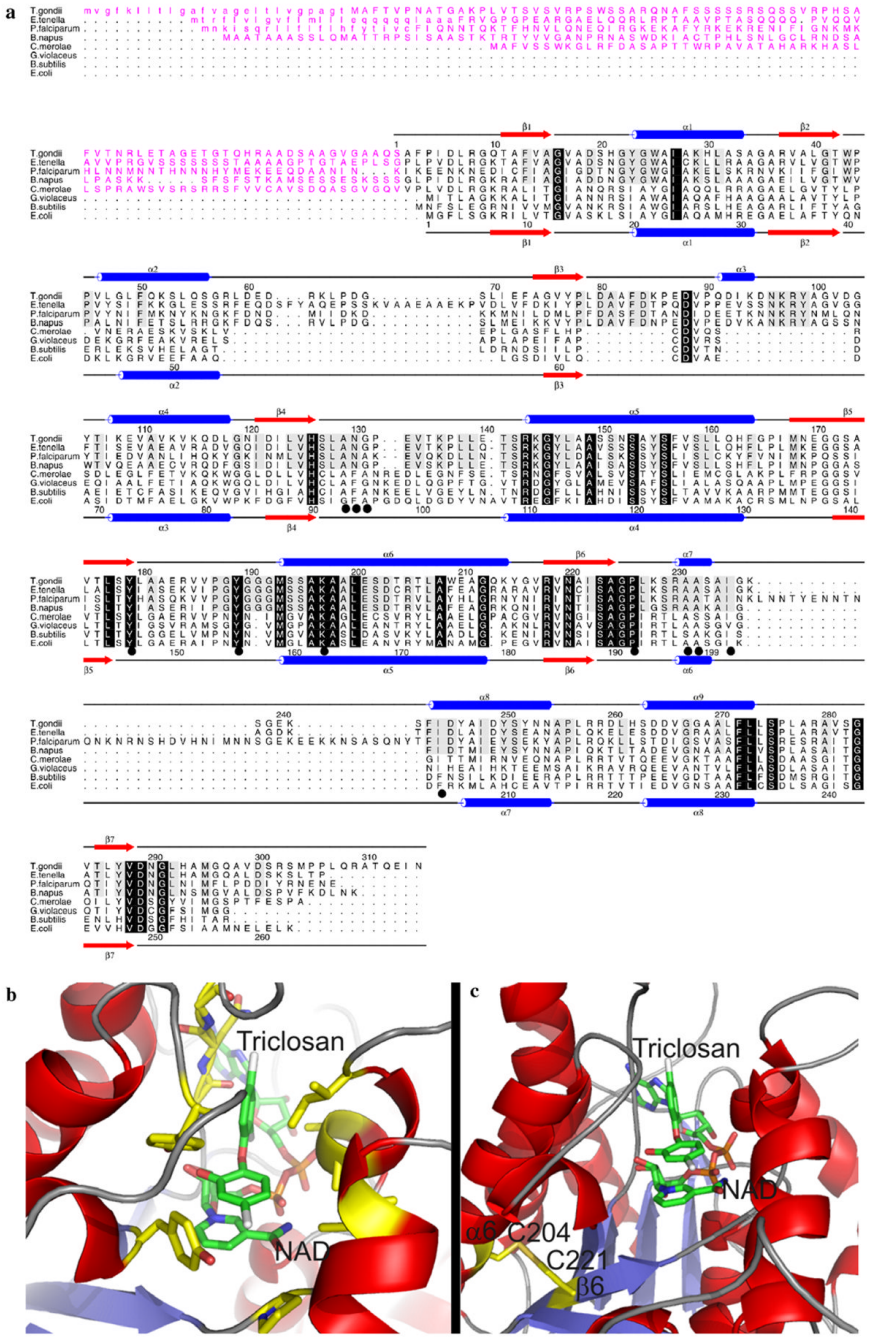

Fig. 1.

(a) A structure-based sequence alignment of ENRs from *Toxoplasma gondii*, *Eimeria tenella*, *Plasmodium falciparum*, *Brassica napus*, *Gloeobacter violaceus*, *Cyanidioschyzon merolae*, *Bacillus subtilis* and *Escherichia coli*. The secondary structure elements and sequence numbering for *T. gondii* and *E. coli* ENR are shown on the top and bottom of the alignment, respectively, with α-helices displayed as blue cylinders and β-sheets as red arrows. Those residues which are conserved across the ENR family are highlighted by a black box with reverse type, with those residues conserved among the apicomplexans being boxed in grey. Those residues which have been shown to be involved in triclosan binding are underscored by a black circle. The transit peptides are shown in purple and the predicted cleavable von Heijne signal

sequences are shown in lower case. (b) The structure of *T. gondii* ENR onto which the residues for *E. tenella* ENR were mutated (in silico) based on the structural alignment in A with those residues involved in triclosan binding (which are fully conserved between *T. gondii* ENR and *E*tENR) shown in a stick format and highlighted by a black circle in the alignment in (a). (c) A structural representation of the position of two2 Cys residues on α6 and β6, which are within the appropriate distance for disulphide bond formation. For both (b) and (c) the stick representations are coloured red, blue, orange, gold and grey for oxygen, nitrogen, phosphorous, sulphur and chlorine, respectively, with carbon being coloured green for NAD^+ and triclosan and yellow for all other residues.

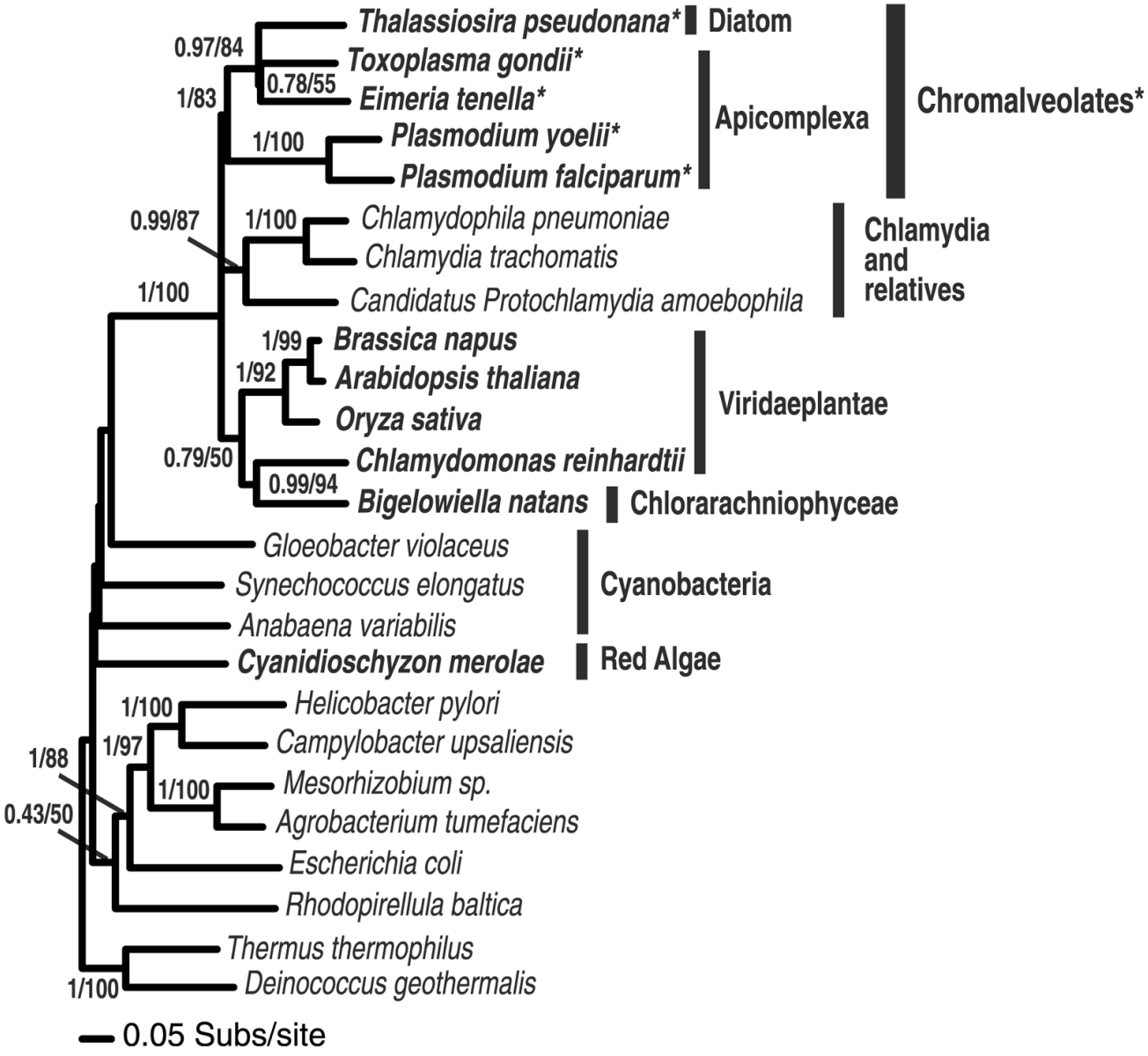

Fig. 2.

Phylogeny of chromalveolate enoyl reductase genes. The chromalveolates cluster strongly with Viridaeplantae, *Chlamydia* and a Chlorarachniophyte gene. Chlorarachniophyte possess a plastid obtained from the secondary endosymbiosis of a green alga. The phylogeny is calculated from an alignment of 25 sequences and a sampling of 217 characters and is arbitrarily rooted in the eubacteria. Eukaryotic taxa are shown in bold. Topology support values are shown in the order posterior probability from a MRBAYES analyses and % bootstrap support from 1000 PHYML bootstrap replicates both using the WAG + Γ + I model. Chromalveolate taxa with shared insertion are marked*.

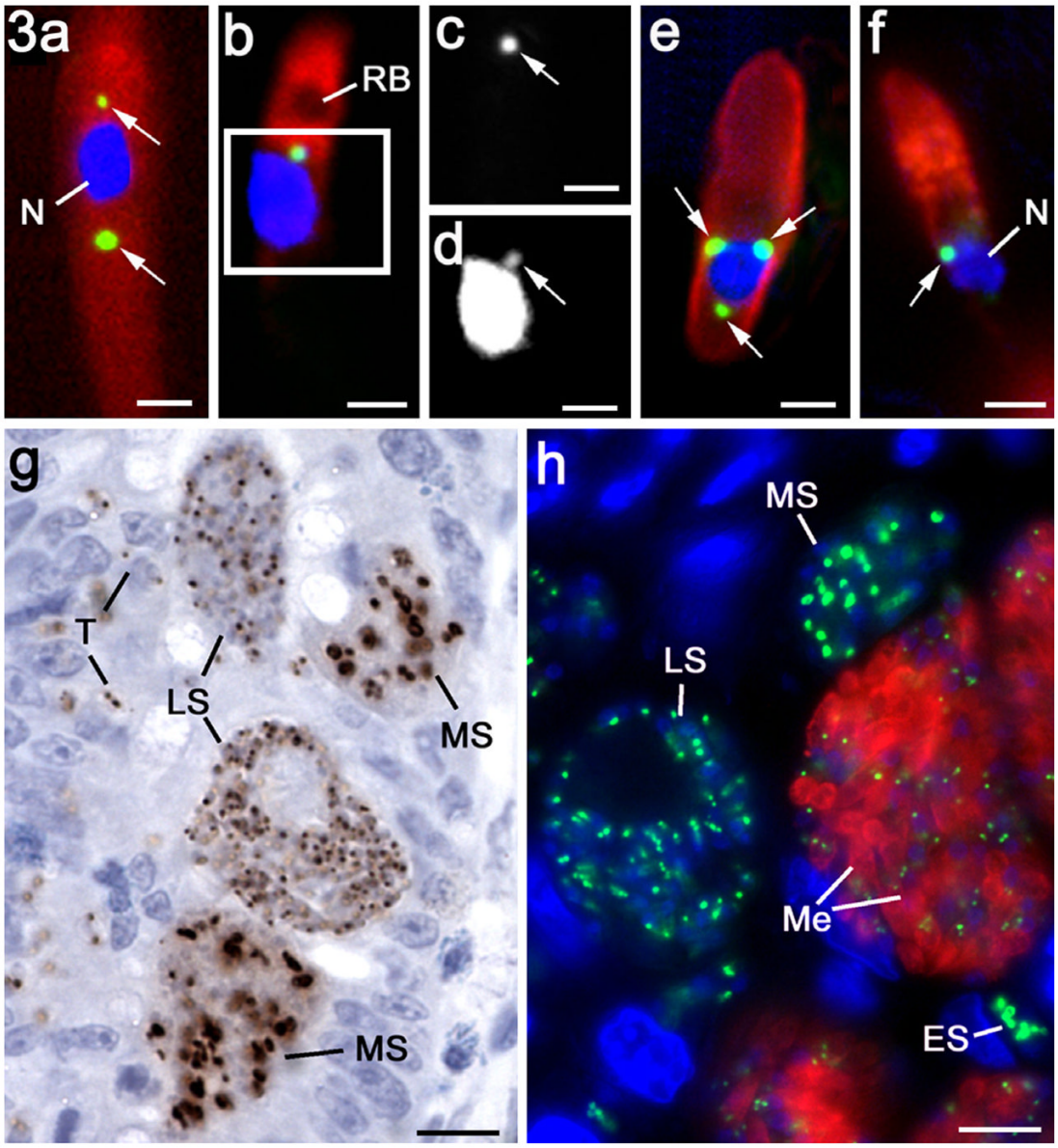

Fig. 3.

Immunofluorescent (a–f, h) and immuno-peroxidase (g) images of various asexual stages of *Eimeria tenella* labelled with anti-*Et*ENR visualised with fluorescein isothiocyanate (green) or DAB/H_2O_2 (brown). The nuclei have been counter stained with 4′,6-diamidino-2-phenylindole (DAPI). Bars represent 1 μm in a–e and 10 μm in g and h. (a) Sporozoite showing two *Et*ENR positive apicoplasts (arrows) either side of the nucleus (N). (b) Sporozoite with a single apicoplast (green) anterior to the nucleus. The micronemes in the anterior are labelled with anti-*Et*MIC2 (red), which outlines the anterior refractile body (RB). (c) Detail of the green channel for the enclosed area in b showing the strong labelling of the apicoplast with anti-*Et*ENR (arrow). (d) Grey level detail from the blue channel showing DAPI staining of the apicoplast (arrow) adjacent to the strongly staining nucleus. (e) Merozoite for the gut lumen showing the surface labelling with anti-*Et*SAG4 (red) and three *Et*ENR positive (green) apicoplasts (arrows) around the nucleus (blue). (f) Merozoite showing the apical labelling of the micronemes with anti-*Et*MIC2 (red) and the *Et*ENR positive apicoplast (arrow) adjacent

to the nucleus (N). (f) Section of the caecum at 48 h p.i. showing mid stage (MS) first generation schizonts with a number of large irregular shaped *Et*ENR positive (brown) structures and late stage (LS) schizonts with numerous small spherical *Et*ENR positive apicoplasts. In addition, a number of small newly entered parasites (T) with one or two small *Et*ENR positive apicoplasts were also located within the epithelial cells. (h) Section of caecum at 112 h p.i. illustrating various stages of schizogony from the early stages (ES) with a few large *Et*ENR positive structures through the mid stages (MS) with a number of large *Et*ENR positive structures to the late stage (LS) with numerous small *Et*ENR positive apicoplasts and finally the mature schizonts with fully formed merozoites (Me) characterised by the labelling with anti-*Et*MIC2 (red), which contain small apicoplasts (green).

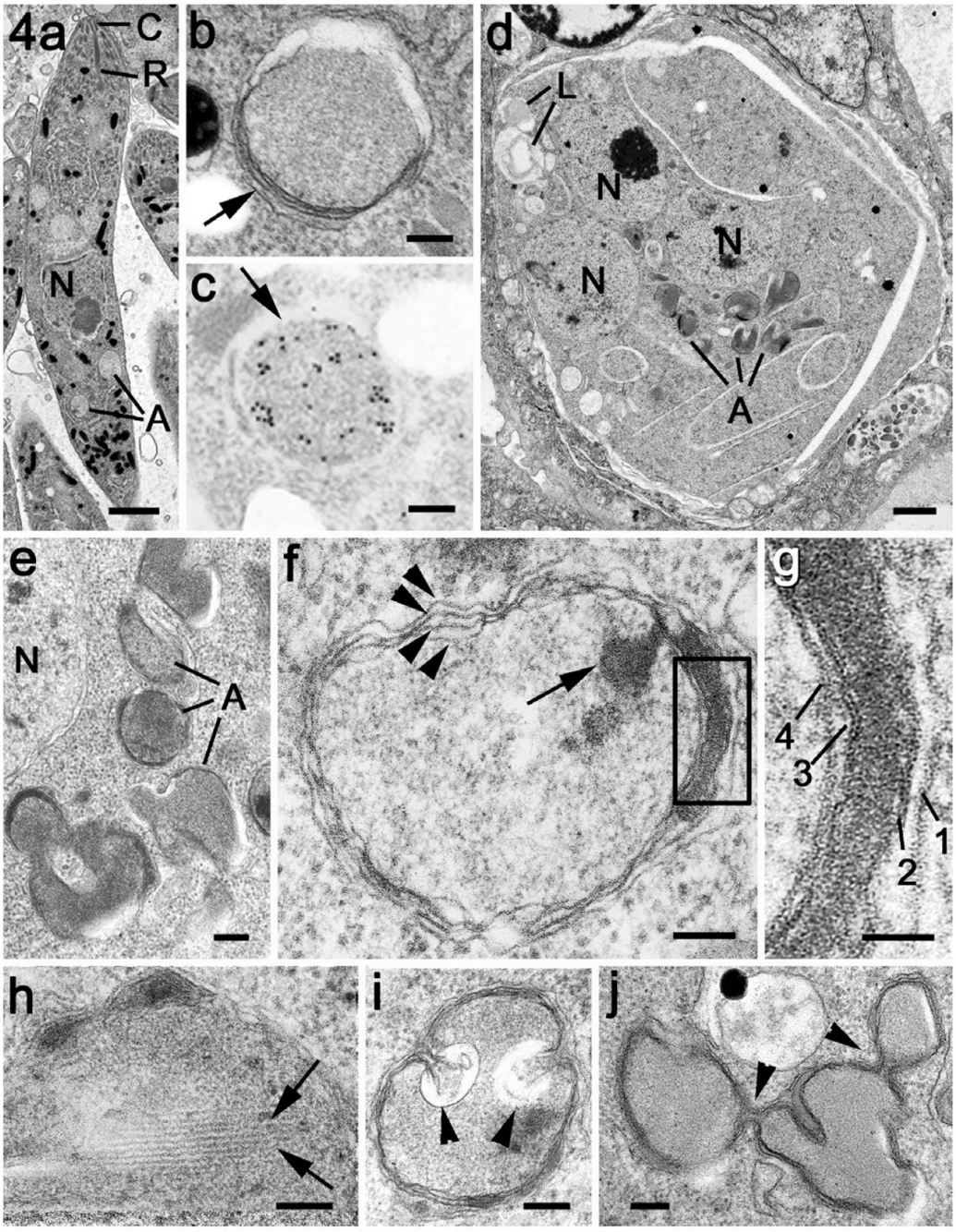

Fig. 4.

Electron micrographs of the apicoplast in the merozoite and during early development of the schizont. (a) Low power of a mature merozoite showing the apical organelles (conoid – C, rhoptry – R) the centrally located nucleus (N) and basely located apicoplasts (A). Scale bar = 1 μm. (b) Detail of the apicoplast from a merozoite showing it to be enclosed by multiple membranes (arrows) with fine granular contents. Scale bar = 100 nm. (c) Immunoelectron microscopy of section labelled with anti-*Et*ENR showing numerous gold particles located over the apicoplast. Scale bar = 100 nm. (d) Low power view of an early schizont which contains a number of nuclei (N) and a few lipid droplets (L). Note the group of electron dense profiles representing the apicoplasts (A). Scale bar = 1 μm. (e) Enlargement of a group of apicoplasts

with fine moderate electron dense contents lying adjacent to a nucleus (N). Scale bar = 100 nm. (f) Detail of an apicoplasts showing areas where the four limiting membranes can be resolved (arrowheads). Note the presence of a plaque of electron dense material within the membranes and also dense material within the lumen of the apicoplast (arrow). Scale bar = 100 nm. (g) Enlargement of the enclosed area in f showing that the electron dense plaque is specifically located between the second and third membranes. Scale bar = 50 nm. (h) Detail of an apicoplasts illustrating the presence of parallel filaments (arrows) within the granular material of the lumen. Scale bar = 100 nm. (i) An apicoplast in which there are invaginations of the membranes (arrowheads) that could relate to apicoplast division. Scale bar = 100 nm. (j) Example of an elongated apicoplast with multiple constrictions (arrowheads), which could represent sites of apicoplast division. Scale bar = 100 nm.

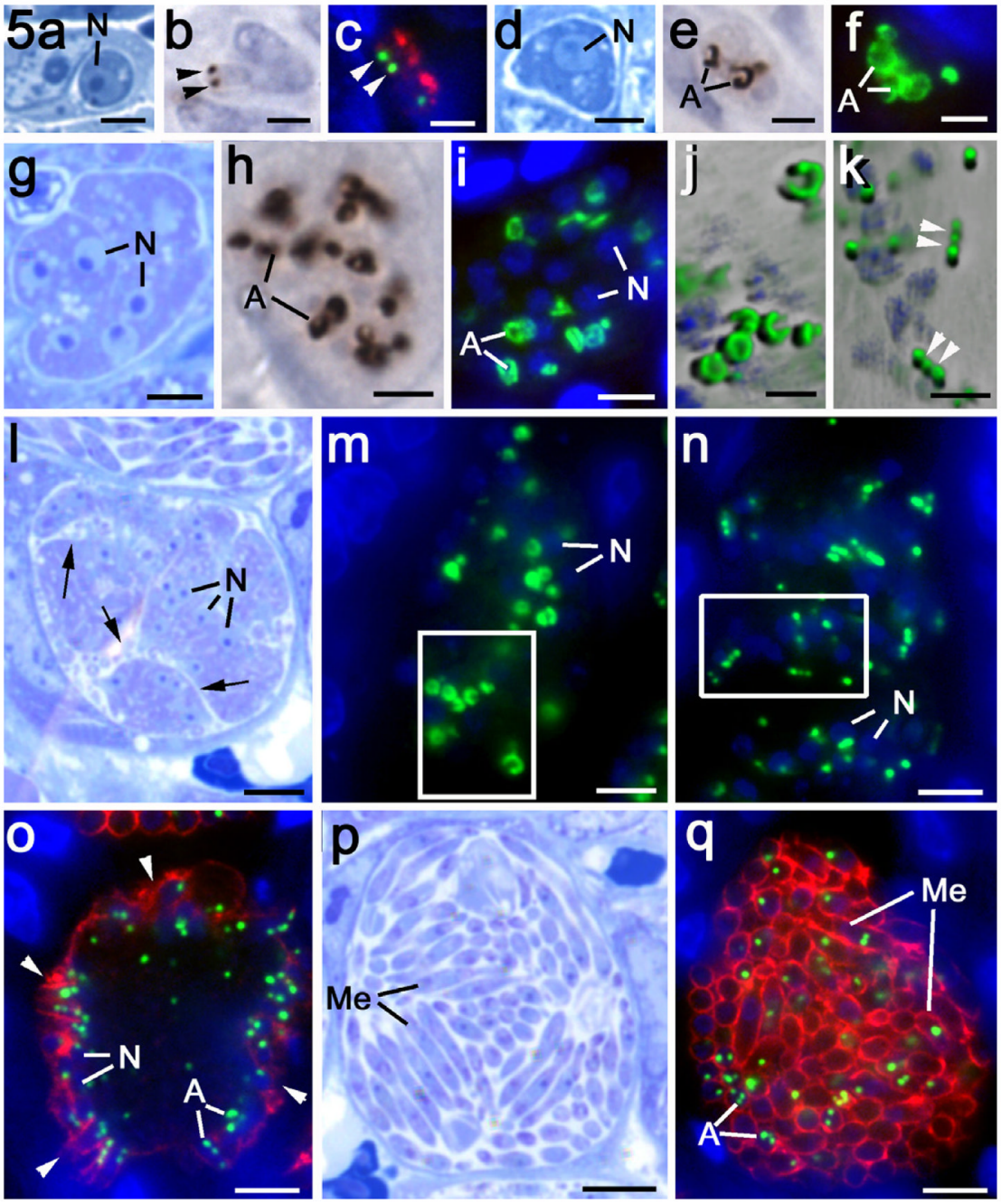

Fig. 5.

Details of the asexual multiplication of *Eimeria tenella* in the chicken caecum observed in plastic sections after staining with azure A (a, d, g, l and p), after immunoperoxidase staining with anti-*Et*ENR (b, e and h) and double labelling with anti-*Et*ENR (green) and anti-*Et*MIC2 (red) (c and f) or anti-*Et*SAG4 (red) (i, m, n, o and q). Scale bars = 1 μm (a–f, j and k), 5 μm (g–i) and 10 μm (l–q). (a–c) Early stage of newly entered merozoites showing two small apicoplasts (arrowheads) with some residual anti-*Et*MIC2 staining (red). (d–f) Early growth stage in which there is marked expansion of the size and signal from the apicoplasts (A). (g–i) Mid-stage with repeated nuclear division resulting in numerous nuclei. Note the increased number of large pleiomorphic-shaped *Et*ENR positive apicoplasts (A). (j) Deconvoluted

enlargement of the enclosed area in m showing the donut and crescentic shape of the large apicoplasts. (k) Deconvoluted enlargement of the enclosed area in n showing repeated constrictions (arrowheads) along the enlarged apicoplasts and the formation of small spherical apicoplasts. (l) Late schizont with numerous nuclei (N) and deep invaginations of the plasmalemma (arrows) increasing the surface area of the schizont. (m) Similar stage to that in l showing a number of randomly distributed large apicoplasts (green). N – nucleus. (n) Slightly later stage than in m showing the apicoplasts as elongated structures with a bead-like appearance and numerous small apicoplasts. The surface of the schizont is still negative for *Et*SAG4 at this stage. N – nucleus. (o) Late stage in schizogony showing the initiation of daughter formation identified by *Et*SAG4 positivity (red) at the schizont surface. Note the nuclei (N) and small apicoplasts (A) have become peripherally located. (p) Mature schizont consisting of numerous fully formed merozoites (Me). (q) Mature schizont showing the fully formed merozoites (Me) outline by the *Et*SAG4 staining (red) and containing one to three small apicoplasts (A).

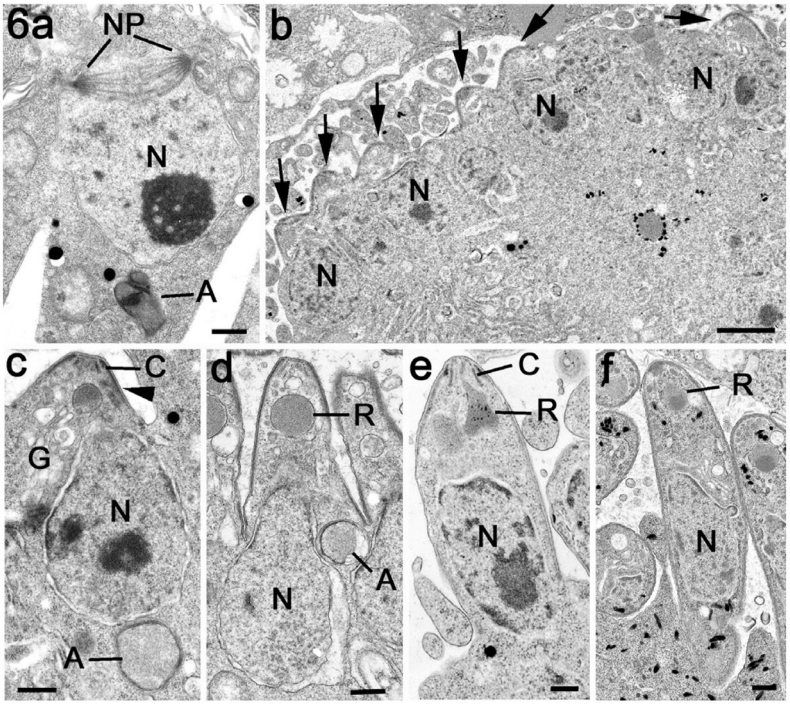

Fig. 6.

Electron micrographs illustrating the later stages in schizogony with formation of the merozoites. (a) Section through a nucleus (N) in a late schizont. Note the absence of apicoplast-like structures associated with the poles (NP) of intranuclear spindle but an apicoplast (A) is located on the opposite side of the nucleus. Scale bar = 500 nm. (b) Low power through part of the periphery of a late schizont showing the peripherally located nuclei and the conical restructures at the plasmalemma representing the initiation of daughter formation (arrows). Scale bar = 1 μm. (c) Detail of the very early stage of merozoites formation showing the conoid (C) and electron dense inner membrane complex of the daughter (arrowhead) budding into the lumen of the parasitophorous vacuole. Note the nucleus associated with the forming daughter and the basally located apicoplast (A). G – Golgi body. Scale bar = 200 nm. (d) A more advanced stage of daughter formation with continued growth into the parasitophorous vacuole. There is the initiation of rhoptry formation (R) and the nucleus (N) and apicoplast (A) are partially within the developing daughter. Scale bar = 200 nm. (e) Later stage with the nucleus (N) within the developing daughter and the rhoptry (R) has a partially developed duct. C – conoid. Scale bar = 200 nm. (f) Fully formed daughter budding from the surface of the schizont. N – nucleus; R – rhoptry. Scale bar = 200 nm.

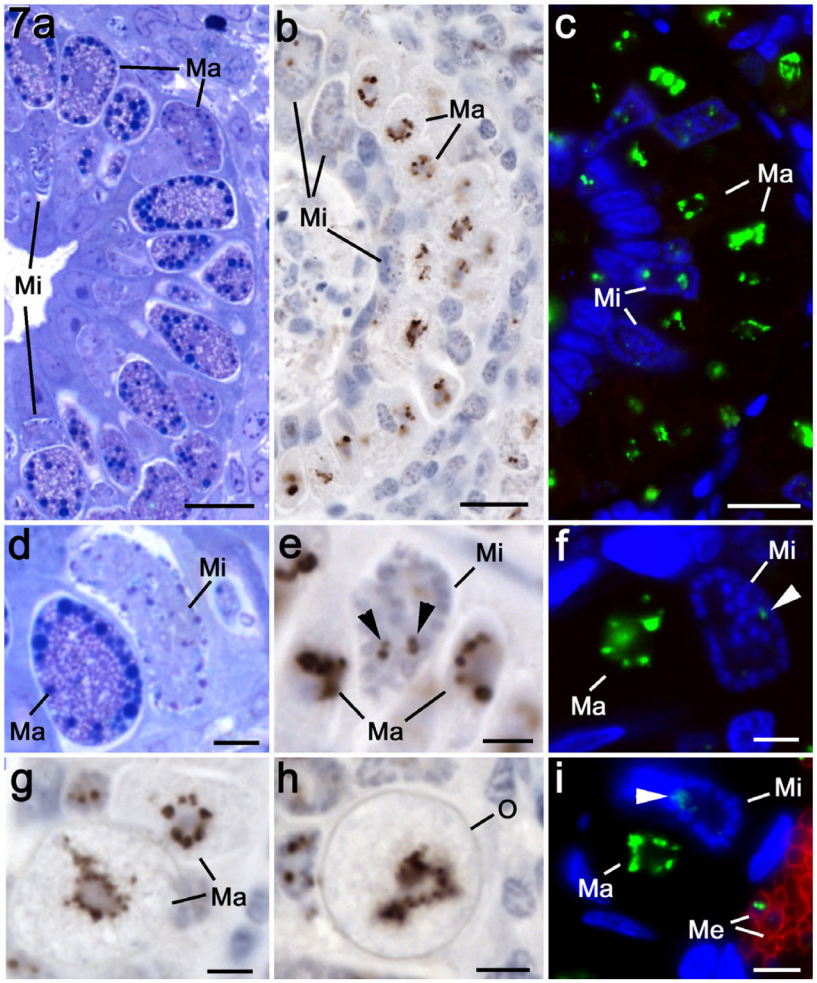

Fig. 7.

Details of the changes in the apicoplast during sexual development using plastic sections stained with azure A (a and d), immunoperoxidase using anti-*Et*ENR visualised with DAB/H2O2 (b, e, g and h) and double-labelled immunofluorescence using anti-*Et*ENR visualised with fluorescein isothiocyanate (green) and anti-*Et*SAG4 visualised with Texas red (red) (c, f and i). Scale bar = 10 μm in a–c and 1 μm in d–i. (a–c) Lower power images through the caecum of a chicken at 142 h p.i. in which numerous stages of microgametogony (Mi) and macrogametogony (Ma) can be seen. Note the large *Et*ENR-positive structures adjacent to the nucleus at all stages of macrogametogenesis and the few small *Et*ENR-positive apicoplasts associated with the developing microgametocytes. (d) Detail showing a late macrogametocyte (Ma) with numerous cytoplasmic granules and wall forming bodies and a mid stage microgametocyte (Mi) with numerous small dense nuclei located towards the periphery. (e) Similar stage to that in d showing macrogametocytes (Ma) with large strongly *Et*ENR positive apicoplasts compared to the small apicoplasts present in the microgametocyte (Mi). (f) Similar stage to that in d showing the strongly staining apicoplast with the macrogametocyte (Ma) and the weakly staining structure (arrowhead) within the microgametocyte (Mi). Neither sexual stage is stained with anti-*Et*SAG4. (g) Mature macrogametocytes (Ma) showing the *Et*ENR positive apicoplasts as lobated or multiple structure. (h) Early oocyst identified by oocyst wall formation (O) showing a large *Et*ENR positive structure centrally located within the oocyst. (i) Similar section to that in f showing the large apicoplast within the macrogametocyte (Ma)

and a small positive structure (arrowhead) within the microgametocyte (Mi). Note the adjacent merozoites (Me), which are positively stained for *Et*SAG4 (red) and contain small apicoplasts.

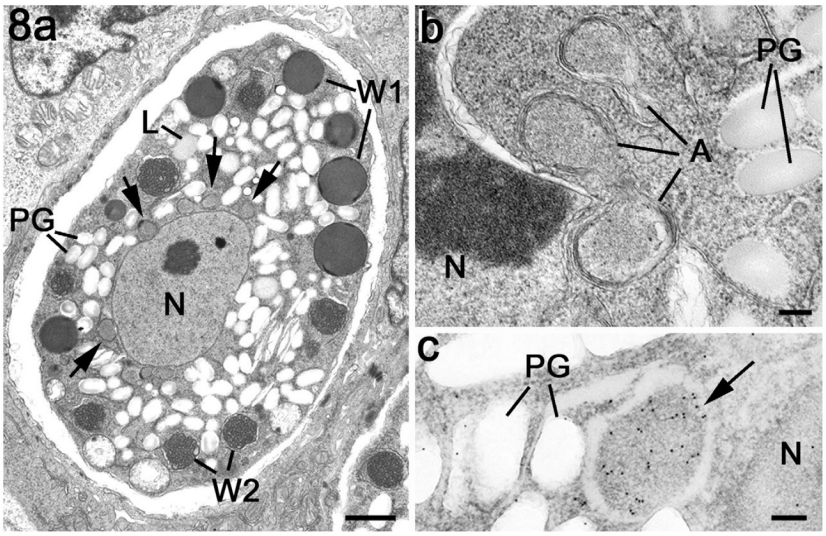

Fig. 8.

Electron micrographs of apicoplasts within the macrogametocyte. (a) Mature macrogametocyte showing the centrally located nucleus (N) with the cytoplasm containing peripherally located wall forming bodies type 1 (W1), wall forming bodies type 2 (W2), numerous lipid droplets (L) and polysaccharide granules (PG). Note the membrane-bound structures representing the apicoplasts around the nucleus (arrows). Scale bar = 2 μm. (b) Detail from the periphery of a nucleus (N) showing a number of profiles of the apicoplast. PG – polysaccharide granules. Scale bar = 100 nm. (c) Immunoelectron microscopy of a section through a macrogametocyte labelled with anti-*Et*ENR showing numerous gold particles over the apicoplast (arrow) located between the nucleus (N) and the polysaccharide granules (PG). Scale bar = 100 nm.

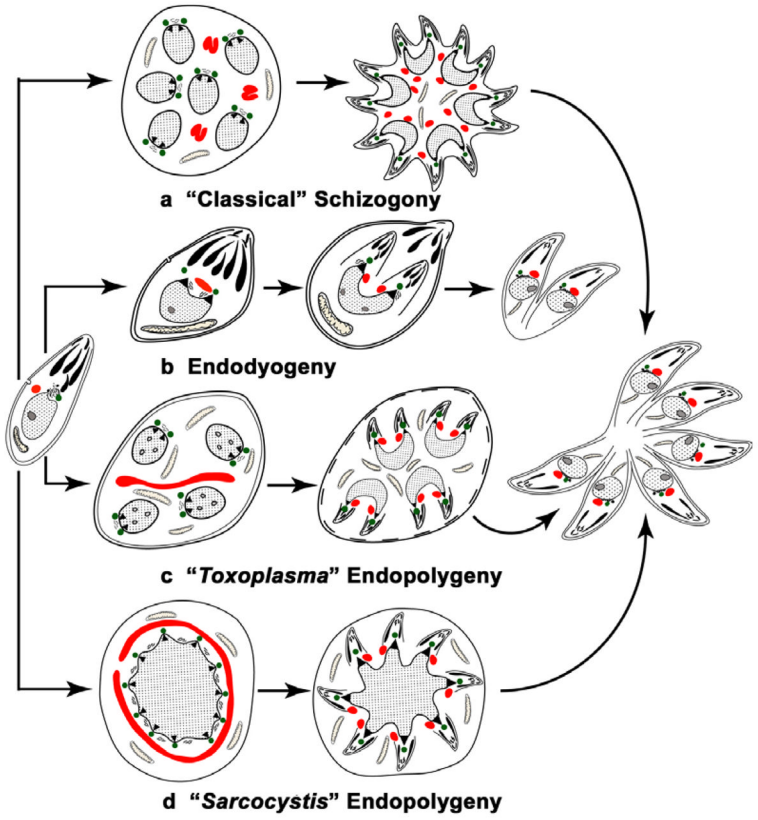

Fig. 9.

Diagram illustrating the differences in the timing and location of nuclear division and daughter formation associated with asexual development within the Apicomplexa. There are four distinct processes: (a) "Classical" schizogony undergone by the majority of apicomplexans, including the genera *Plasmodium* and *Eimeria*, where there is a proliferative phase with repeated nuclear divisions followed by a differentiation phase with daughter formation initiated at and budding from the parasite plasmalemma. (b) Endodyogeny in which there is no proliferative phase, but one cycle of DNA replication with the initiation of the formation of two daughters within the mother cell cytoplasm prior to the completion of nuclear division. (c) "*Toxoplasma*" endopolygeny, used to describe the asexual division of *Toxoplasma gondii* in the definitive host, involves a proliferative phase with repeated nuclear division, similar to "classical" schizogony, but differs in that daughter formation is initiated within the cytoplasm in a similar manner to endodyogeny. (d) "*Sarcocystis*" endopolygeny has been reported for certain *Sarcocystis* species and involves an initial phase with repeated cycles of DNA replication and formation of numerous nuclear spindles, but no division of the nucleus. Formation of multiple daughters is initiated within the cytoplasm and the large polyploidy nucleus fragments and one haploid nucleus enters each developing daughter. In the diagram, centrioles are represented by green circles, apicoplasts by red structures and nuclear poles by black triangles.

Table 1

Predicted dynamin, MinD and Centrin proteins found in the *Eimeria tenella* genome project share similarity to a wide variety of organisms

E. tenella **predicted protein**	**Organism with closest sequence similarity (gene description)**	**Accession number of published sequence**	**Probability**
Dynamin Eimer_2900c04.plk	Dictyostelium discoideum (Dynamin like protein)	XP_642112	3e-54
	Homo sapiens (Dynamin 3)	NP_056384	2e-53
	Arabidopsis thaliana (Dynamin like protein)	AAM61220	2e-49
MinD Eimer_2796f01.qlk	*Cryptosporidium parvum* (MRP like MinD family ATPase)	EAK88253	3e-11
	Clostridium acetobutylicum (MinD family ATPase)	AEO07795	3e-09
Centrin1 Eimer bac 47a4Ef12.qlk	*Plasmodium falciparum* (Centrin putative)	NP_702332	8e-51
	Paramecium tetraurelia (Centrin putative)	CAH03655	1e-41
	Tetrahymena thermophilia (Centrin)	AAF66602	3e-35
	A. thaliana (Centrin)	CAB62315	2e-28
Centrin2 Eimer bac 47a4Ef12.qlk	*Ochromonas danica* (Centrin)	BAD20712	6e-43
	Giardia intestinalis (Centrin)	AAC47395	3e-39

The organisms with closest sequence similarities for each of the organellar division proteins and the accession numbers of the proteins or predicted proteins are provided. The role of these proteins in organellar (plastid, mitochondrial or nuclear) division remains to be determined.